JAST, Vol. 14, No 1, pp 91-102

JAST
Journal of Aerospace Science and Technology

Science Article

Critical Cavitation Number Determination of a High-speed Centrifugal Pump by Numerical Simulation of a Two-phase Flow

Ali Cheraqi[1]*, Reza Ebrahimi[2]
1-2- Combustion and Propulsion Research Laboratory, Faculty of Aerospace Engineering, K.N.Toosi University of Technology, Tehran
*Tehran, Daneshgah Boulevard, Ehsan Street Exit, East Zeynoddin Highway
Email: *Cheraqi@email.kntu.ac.ir

This paper aims to present an investigation on determining the critical cavitation number of a high-speed centrifugal pump by computational fluid dynamics. In doing so, characteristic curves of the pump used in this study were obtained in the presence and absence of cavitation. The critical cavitation number was calculated based on the cavitation breakdown characteristic curve. Two-phase flow inside the pump was simulated using the homogenous mixture method and the Rayleigh-Plesset model. The SST turbulence model and MRF rotating model were used to simulate turbulence and rotation of the flow throgh the pump, respecively. The critical cavitation number that was the outcome of numerical analysis results was compared to the experimental data. This comparison implied the necessity of considering the safety factor for determining the critical cavitation number and inlet pressure required to uninterrupted operation of the pump cavitation, using the results of numerical analysis.

Keywords: *centrifugal pump, the critical cavitation number, inducer, CFD, the characteristic curve*

Introduction

Cavitation is a dynamic process seen in centrifugal pumps involving the formation, growth, and collapse of cavities in a fluid passing through blades. Depending on the flow conditions, different types of cavitation can be seen in the centrifugal pumps, including backflow cavitation, blade cavitation, bubble cavitation and tip vortex cavitation and other types of cavitations.

At this point, we should point out that cavitation is generally an extremely damaging phenomenon, and that its harmful consequences can be divided into three categories. First, it can cause damage to the material surfaces near the region where bubbles collapse. costly damages of cavitation is the challenging problem associated with cavitation. Complete elimination of cavitation is frequently aimed to be achieved. However, in most circumstances, it is impossible to eliminate cavitation completely, so the effort must be focused on minimizing the adverse effects of this phenomenon.

Secondly, cavitation can significantly degrade the performance of the pump or other hydraulic devices. In pumps, there is a phenomenon called cavitation breakdown in which the performance significantly declines at a certain level of inlet pressure. It is necessary to design a pump with proper suction function in order to prevent

1 PhD Student (corresponding author)
2 professor

Received: 18 August 2021
Accepted: 17 Oct. 2021

performance drop in cavitation conditions. One way to prevent cavitation is to add a inducer upstream of the impeller in high-speed centrifugal pumps. Proper design of the blade profile, the shape of the leading edge and its sharpness are other methods to prevent or reduce the occurrence of cavitation in pumps.

The third adverse effect of cavitation is not widely known and derives from the fact that cavitation affects not only the steady-state fluid flow, but also the unsteady or dynamic response of the flow. This change of dynamic performance causes instabilities in the flow that do not occur in the absence of cavitation. Examples of such instabilities are rotating cavitation, which is somewhat similar to the rotating stall phenomenon in a compressor, and auto-oscillation, which is to some extent identical to compressor surge. These instabilities can raise oscillating flow rates and pressures that can damage the structural integrity of the pump or its inlet or discharge ducts. Although an inclusive classification of the various types of unsteady flow caused by cavitation has yet to be developed, we can nevertheless identify some specific types of instability.[1]

These cavitation effects shed light on the importance of obtaining pumps' characteristic curves in the absence and presence of cavitation. The characteristic curve of a non-cavitating conditions is called performance characteristic curve or H-Q curve. The characteristic curve of a cavitating conditions is called the cavitation breakdown curve. experiments is the most accurate method to extracte characteristic curves, but these are very expensive. In this paper the flow in a high speed centrifugal pump is simulated to evaluate characteristic curves. First, the characteristic performance curve of the pump under non-cavitating conditions was extracted and validated with available experimental and analytical data. Then, the flow under cavitating conditions was simulated to obtain the cavitation breakdown curve and the critical cavitation number.

Centrifugal pumps transfer energy to the fluid and are among a system's active elements that play a crucial role in the system's dynamic. Although there is a comprehensive survey of scholarly sources on pump performance in a steady state, little attention has been paid to pump performance in a flow oscillation state. This becomes even more complicated when the pump is in a two-phase flow and cavitation condition. Therefore, studying the performance of pumps in cavitation conditions is essential both in terms of predicting critical cavitation and in terms of studying dynamic behavior. Cavitation flow simulation methods can be classified into two general categories.

The first method is a numerical method based on the potential flow theory and is used to determine the vapor region by tracking the boundary of vapor-liquid interface. This method assumes a fixed vapor pressure for the liquid in the secondary vapor phase. So, the boundary of vapor-liquid interface is traceable and the shape of the cavity is formed through an iteration of a process. This first method is a physics-related theory that has been proved by experiments and is used for sheet cavitation modeling but is not suitable for cavity growth or separation. However, since tracking the boundaries of the interface is demanding in three-dimensional flows, this method has been limited to simulating two-dimensional and axisymmetric flows.

The second method includes the multiple-phase mixture model or homogeneous equilibrium model. These models use a same kind of fluid to model a two-phase flow but are different in determining the density field.

Literature review

Coutier-Delghosa et al. (2002) conducted a numerical study of the effect of the leading edge shape on cavitation around inducer blade sections. They used two-dimensional hydrofoils for simulating a cavitating flow on an inducer blade. Two leading-edge shapes were chosen to approach liquid rocket engine inducer designs. The numerical model of cavitating flows was based on the three-dimensional code FINE/TURBOTM. The cavitation process was studied using a single fluid model in which liquid vapor mixtures were considered homogeneous fluids whose density varied in relation to static pressure. Numerical results were compared with experimental ones. The influence of the leading edge shape on the cavitation behavior was examined. [2]

Tokumasu et al. (2004) ran a numerical analysis on the effect of flow properties on the thermodynamic effect of cavitation. By decreasing temperature, latent heat of vaporization lowers the vapor pressure and suppresses cavity growth. This is called the thermodynamic effect of cavitation. This effect is especially significant in cryogenic fluids such as LOX and LH2. Tokumasu et al.

numerically estimated the size of the cavity in a cryogenic fluid by taking account of the thermodynamic effect of cavitation. Based on the results, the thermodynamic effect of cavitation was investigated according to liquid and Reynolds number properties. [3]

Ugajin et al. (2006) simulated an unsteady cavitating flow in a turbopump inducer using a three-dimensional detached eddy simulation (DES) code. The cavitation was modeled by the source/sink of the vapor phase in the liquid flow. The computational results were compared with experimental measurements, and good agreements with experiments were concluded. The unsteady motions of cavities were simulated in the inducer. The magnitude of the oscillation in cavity volume increased as the cavities extended and blocked the throat of the flow passage. The effect of the tip-gap on the cavity volume was shown; the time-averaged volume of cavities for the inducer with the tip-gap is about five times larger than that for the inducer without the tip-gap. However, their work did not examine unsteady phenomena such as rotating cavitation and cavitation surge in the inducer. [4]

D. Pierrat et al. (2008) conducted an experimental and numerical investigation of leading edge cavitation in a helico-cebtrifugal pump. In their study, the leading edge cavitation was experimentally observed on the both sides of the impeller and the head drop measured for different operating conditions. A CFD model for cavitation simulation was employed and compared to experimental results for 3 flowrates, ranging from 0.85 Qn to 1.25 Qn. There was a good agreement between the cavitation figures obtained from numerical analysis and those from experimental analyses. [5]

Yamamoto and Tsujimoto (2009) investigated the effects of backflow vortex cavitation on cavitation instabilities. Cavitation instabilities in turbo-machinery, such as cavitation surge and rotating cavitation, are usually attributed to the quasi-steady characteristics of cavitation, mass flow gain factor and cavitation compliance. However, there are certain cases when it is necessary to take account of unsteady characteristics. In order to demonstrate the importance of the phase delay of backflow vortex cavitation, a cavitation surge in industrial centrifugal pumps was presented as an example. They first outlined the fundamental characteristics of the backflow vortex structure and then discussed the energy transfer under cavitation surge in the centrifugal pump. Finally, they discussed the dynamics of backflow to explain a significant phase lag observed in the experiment. [6]

Kang and Yonezawa (2009) investigated cause of cavitation instabilities in a three-dimensional inducer. Alternate blade cavitation, rotating cavitation and cavitation surge in rocket turbopump inducers were simulated by a commercial code. Towards clarifying how cavitation instabilities occur, the velocity disturbance caused by cavitation was obtained by subtracting the velocity vector under non-cavitating conditions from the one under cavitating conditions. They found that an axial component of the disturbance flow towards downstream reduces the incidence angle towards the next blade at the trailing edge of the tip cavity. It was found that all of the cavitation instabilities emerge when this disturbance flow starts to interact with the leading edge of the next blade. Experiments have confirmed the existence of a disturbance flow. [7]

An and Shin (2011) numerically examined vortices behavior of the internal flow through a centrifugal pump including formation and shedding of cavitation. Structured mesh was used to compute a three-dimensional flow inside a single section centrifugal pump with six blades. A constant suction vortex was applied as a boundary condition. Two pump systems with and without suction vortices were studied in relation to the variation of flow rates. The results showed that suction vortices induced biased flow structure and increased cavitation, particularly at the low flow rate condition. Internal flow phenomena through impellers, including cavitation formation, vortex growth and shedding, flow separation, and flow instability due to suction vortices, were studied and discussed. [8]

Somashekar and Purushotham (2012) numerically simulated cavitation inception on radial-flow pump. They, based on experimental data, presented the validation of cavitation inception on a radial-flow pump which develops 21m of head at 26lps of discharge at its best efficiency point (BEP) of discharge while operating at a speed of 1500rpm. Numerical analyses were run by ANSYS13 and CFX software. The pump's performance characteristic and cavitation breakdown curves were extracted. [9]

Campos-Amezcua et al. (2013) conducted a numerical and experimental study of cavitating flow through an axial inducer considering tip

clearance. They presented three-dimensional numerical simulations and experimental investigations of cavitating flow through an axial inducer. Numerical analysis was done on two different configurations, with particular emphasis on radial tip clearance's influence on cavitation behavior. The first configuration was modeled without considering tip clearance. Then, the inducer was modeled with nominal tip clearance and some modifications of this. It was found that radial tip clearance significantly influences the overall inducer performance in the non-cavitating regime because of the small-sized inducer. Moreover, the effects of radial tip clearance are strong in inducer cavitation behavior. Numerical results and experimental data with nominal tip clearance were compared and discussed in cavitating and non-cavitating regimes.[10]

Mishra and Ghosh (2015) predicted the performance of axial pump inducer of LOX booster turbo-pump of staged combustion cycle-based rocket engine using CFD. Their paper presents a steady-state CFD analysis of the inducer of a liquid oxygen (LOX) axial pump used as a booster pump for an oxygen rich staged combustion cycle rocket engine using ANSYS® CFX. Mishra and Ghosh obtained the performance characteristic curves for the LOX pump inducer. They used the formalism to predict the performance of the inducer for the throttling range ranging from 80% to 113% of nominal thrust and for the different rotational velocities ranging from 4500 to 7500 rpm. Simulations were performed to determine the region of cavitation inception for different inlet pressures. [11]

Guo et al. (2016) studied the manner in which the number of inducer blades can affect the anti-cavitation characteristics and external performance of a centrifugal pump. They first used the Rayleigh-Plesset equation and the mixture model to simulate the vapor liquid flow in a centrifugal pump with an inducer, and then predicted its external performance. Finally, they tested the external performance of a centrifugal pump with 2-, 3- and 4-bladed inducers, respectively. They experimented with the three cases and validated their numerical results. They discovered that the vapor volume fraction of a centrifugal pump with a 3- bladed inducer is less than that of a centrifugal pump with 2- or 4-bladed inducers, meaning that a centrifugal pump with a 3-bladed inducer has a more efficient external and anti-cavitation performance. [12]

Cheraqi and Ebrahimi (2021) simulated a flow in a high-speed centrifugal pump to determine its range of steady performance. Experimental and analytic data validated numerical results. Simulations were performed with a wide range of flow coefficients. They ran a single-phase analysis on flow. [13]

In the present study, the performance characteristic curve of a high-speed feed pump in the presence of cavitation in a two-phase fluid was extracted by computational fluid dynamics. The components of the pump used during the study are shown in Figure 1, including a two-blade inducer, a six-blade impeller and a single-volute casing.

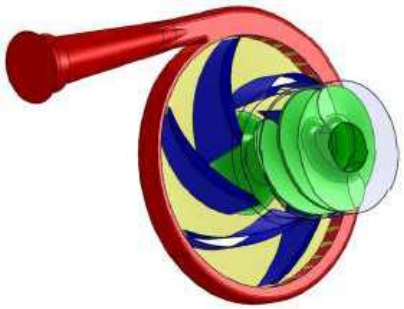

Figure 1 – Structure of the pump including inducer, impeller and volute

The inducer was implanted to increase inlet pressure into the impeller and prevent the presence of cavitation in the eye. The volute was implemented to recall the discharge pressure from the impeller. Cheraqi and Ebrahimi (2021) validated the numerical analysis results of this pump in the absence of cavitation by comparing them with the existing experimental results. [13]

In the present study, a two-phase analysis was run to simulate cavitation and determine the pump's critical cavitation number.

Non-cavitating performance characteristic curve of the pump

Performing experiments is the most reliable way to obtain the non-cavitating performance characteristic curves of a pump. By testing the performance of the pump, in addition to shortcomings of design and manufacturing, the pump's behavior outside of the design point will be predicted. According to the API610 standard, the purpose of these tests is to obtain the pump's performance characteristic curves and determine parameters such as vibrations, flow rate, head and power consumption. However, the pump's head-

flow curve can also be obtained by solving experimental-analytic equations obtained from a large number of experiments on pumps. The pump's operating point should be already determined from experiments to solve these equations. The pump's performance outside the design point is determined by a quadratic equation.

Cavitating performance characteristic curve of the pump

Non-dimensional parameters have been used in research to assess cavitation in pumps. Cavitation number (σ) is the most significant parameter that serves as an indication of cavitation presence. The equation of calculating σ is shown below.

$$\sigma = \frac{p_{in} - p_v}{\frac{1}{2}\rho(r_{t1}\omega)^2}$$

Pin represents inlet pressure, p_v represents vapor pressure, p represents water/liquid density, r_{t1} represents the radius of tip blade of inducer, and ω denotes the pump's rotating speed.

The more the cavitation number decreases, the more the possibility of cavitation presence in the pump increases. According to the above formula, the cavitation number of a given pump with a specified fluid decreases with the decrease of inlet pressure and increase of pump's operating speed. Depending on the value of σ, cavitating flows of pumps fall into the following categories.

1. Incipient cavitation
   This stage of cavitation involves creating and collapsing bubbles, is blaring, and often causes damage to solid surfaces. Bubbles are tiny but visible and the cavitation area is limited in this stage. The cavitation number of this stage is called the cavitation inception number.
2. Partial cavitation
   This kind of cavitation occurs when bubbles cover parts of the blades. The cavity is untransparent, beating, pulsating and unstable. The cavitation number in this condition is smaller than the cavitation inception number.
3. Supercavitation
   The smaller the cavitation number becomes, the bigger cavity dimensions grow. The cavity covers many parts of the blades and is transparent and stable in this state.

Pump's cavitation characteristic curves can be obtained through two methods. One is finding the lower limit of cavitation number per fixed flow rate and rotating speed. In this method, the cavitation number is decreased by gradual reduction of inlet pressure of flow rate in pump and maintaining the rotating speed fixed. Cavitation number coinciding with the creation of the first vapor bubbles is called cavitation inception number denoted by σ_i. Cavitation number coinciding with a certain amount of head drop (usually of 2 to 5 percent) is called critical cavitation number denoted by σ_c. Further decrease in the cavitation number leads to a significant drop in the pump's performance. The cavitation number of this condition is called the "cavitation breakdown number" denoted by σ_b.

The second approach determines the upper limit of flow rate per cavitation number and fixed rotating speed. As expected, the higher the flow coefficient, the higher the critical cavitation number. In other words, when the flow rate is high at a certain speed, cavitation occurs at a high inlet pressure. In this method, inlet pressure and rotating speed are maintained fixed but the flow rate is increased gradually and as in the first method is used to assess critical cavitation. [1]

The behavior of fluid dynamics is described by their governing partial differential equations. These equations can not be solved analytically. So, the governing equations are solved by dividing the solution field into smaller cells (i.e., meshing the solution field) and using numerical methods such as finite volume and finite difference methods.

Experiments should validate the performance of systemes like centrifugal pumps after they are designed. Nowadays, the development of computers with strong CPUs and also numerical methods for solving the governing equations on three-dimensional flows and rotating elements has waved away the obstacle of experiments such as their expenses and time-consumingness. So, computational fluid dynamics can be used as a complementary method to experimental methods for validating the design and production and predicting the pump's behavior in points outside the design. The present study used the CFX software to simulate cavitating flow through a high-speed centrifugal pump.

Governing equations

The following are two ways of presenting continuity and momentum equations for a single-phase fluid flow.

$$\frac{\partial \rho}{\partial t}+\frac{\partial}{\partial x_j}(\rho U_j)=0$$

$$\frac{\partial(\rho U_i)}{\partial t}+\frac{\partial}{\partial x_j}(\rho U_i U_j)=-\frac{\partial p'}{\partial x_i}+\frac{\partial}{\partial x_j}\left[\mu_{eff}\left(\frac{\partial U_i}{\partial x_j}+\frac{\partial U_j}{\partial x_i}\right)\right]+S_M$$

S_m denotes resultance of body forces, μ_{eff} denotes the effect of viscosity in turbulence and p' denotes modified pressure. In rotating systems with the fixed angle speed ω, more source expressions are required to calculate Coriolis and centrifugal force.

$$S_M=-2\rho\vec{\omega}\times\vec{U}-\rho\vec{\omega}\times(\vec{\omega}\times\vec{r})$$

The first expression in the above equation results from centrifugal force and the second from Coriolis force.

In the present study, steady simulations were employed. Since the solution field included inlet, inducer, impeller and volute, flow simulation was performed by using static and dynamic coordinate systems simultaneously and employing the Moving Reference Frame model.

There are different models for turbulence simulation in commercial codes. However, there is no integrated model to be used in all turbulent flows. The option of the turbulence model depends on the governing physics, accuracy of computations, the quality of the meshing grid and computational facilities. Two-equation models are more practical and accurate than other models and are compatible with numerical methods and computational accuracy. The $k-\varepsilon$ model is the most common two-equation model. Since the strengths and shortcomings of this model are known, many works have concentrated on optimizing it. Considering that this is a high-Reynolds model, it is inefficient in areas close to the wall (low-Reynolds area).

On the contrary, the $k-\varepsilon$ model is very efficient in predicting the flow behavior near the wall by using dense elements. In order to enjoy the advantages of both models, a mixture of the two models mentioned above has been employed called the SST model. The SST model is more accurate and reliable when there is a flow with an adverse pressure gradient. Although this model enjoys the benefits of both primary models, it may cause instabilities in solution or a weak convergence due to switching from one model to another. 15 Ultimately, we employed the SST model in the present study.

Cavitation model

The current study used the Rayleigh-Plesste model based on the volume fraction transport equation to simulate cavitation in the pump. The fluid during cavitation consists of two phases, including vapor and liquid and three elements, including vapor, liquid and compressible gas. The following equation exists between volume fractions of water denoted by $_w$, vapor denoted by $_v$ and incompressible gas denoted by $_g$.

$$(\alpha_w+\alpha_g)+\alpha_v=1$$

Assuming a no-slip condition for phases and a complete blending of compressible gas with the liquid phase, the equation of liquid volume fraction is presented below.

$$\alpha_l=\alpha_w+\alpha_g$$

And the equation of overall transfer of liquid phase is presented below.

$$\dot{m}_l^v=-F^v\frac{3\alpha_{nuc}(1-\alpha_v)\rho_v}{R_B}$$

Production rate and vapor compressibility during the cavitation process are calculated by the source expressions $\dot{m}^v_l$ and $\dot{m}^c_l$. In other words, these expressions determine mass transfer between phases.

$$\dot{m}_l^v=-F^v\frac{3\alpha_{nuc}(1-\alpha_v)\rho_v}{R_B}\times\sqrt{\frac{2}{3}\frac{|p_v-p|}{\rho_l}}\operatorname{sgn}(p_v-p)$$

$$\dot{m}_l^c=F^c\frac{3\alpha_v\rho_v}{R_B}\sqrt{\frac{2}{3}\frac{|p_v-p|}{\rho_l}}\operatorname{sgn}(p_v-p)$$

Regarding these equations, $R_B=1\times10^{-6}$ m represents the core diameter of cavitation, $a_{nuc}=5\times10^{-4}$ represents the volume fraction of cavitation core, and $F^v=50$ and $F^c=0.01$ denote the research constants. [15]

Computational Domain

The geometry of the pump was generated by SOLID software. For running CFD analysis, the fluid field of the model was determined. The

solution field consisted of a rotating part, including inducer and impeller, and a nonrotating part, including volute, inlet, and outlet ducts. An outlet duct was added to the volute to achieve better convergence of results. In Figure 2, the computational field is shown.

Griding of the solution field was built by Gambit. In order to choose a suitable grid, three different grids with a different number of meshes were generated, and numerical analysis was performed at the performance point. Table 1 shows the specifications of generated grids as well as influential parameters in the quality of meshes of the three grids. Numbers are presented in percentage in this table. Since the head coefficient obtained from analyses on rated point of the second and third grids are not significantly different, the second grid was used for analyzing other performance points in order to reduce the computational costs.

Due to the high number of computations in the present study, we used parallel processing. After meshing and setting the conditions by the MeTiS separator, the solution field was divided into 32 computational areas, and a processor analyzed each area.

Figure 2 – computational domain for flow calculation passing through the pump

Table 1 – Specifications of generated grids numerical for simulation of flow

Grid Type	Element Number	Exp. Factor	Orthog. Angle	Aspect Ratio	Flow Coeff.	Head Coeff.
	Million	Max= 10	Min= 20	Max= 10	Rated	Rated
1	2.824	3.94	4.61	2.23	0.068	0.742
2	5.286	1.97	2.18	1.05	0.068	0.717
3	8.065	0.92	1.25	0.56	0.068	0.718

Results

Cheraqi and Ebrahimi numerically simulated the flow in the pump used in the present study under different mass flow rates. [13] The characteristic curve obtained from this study was compared with the characteristic curve obtained from experimental data and semi analytical. Figure 3 presents the pump's characteristic curves obtained from all three methods. Graphs point out that numerical results are significantly different from experimental ones. Part of this difference is due to simplification of the pump's geometry during building the fluid model. During this stage, some pump elements, including leakage passages, seals, and leakage return passages, were eliminated. Efficiency of the pump increases due to this elimination and consequently skipping over leakage and disk wastages. Another reason for the difference between numerical and experimental results is the solution's accuracy and numerical errors that are inevitable in numerical simulation of fluid flow. Thus, the existing difference between numerical and experimental results is acceptable, and the results of numerical analysis can be counteracted based on the wastages mentioned above. The modified results can be seen in the pump's characteristic curve. We computationally modified the results by reducing the existing difference at the nominal point and applying the wastages of leakage and leakage return passages to the simulation results.

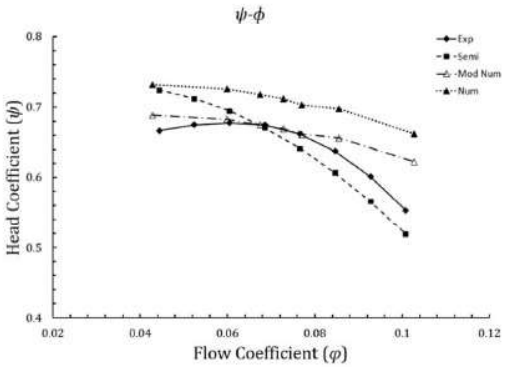

Figure 3 – Characteristic curve of pump and comparison of it with semi-analytical and experimental results [2]

Simulation was done in lower flow coefficients, and the pump's unsteady performance area was determined. The part of the flow coefficient where the curve slope is positive was determined to be the pump's steady performance area. The unsteady area of the pump can be seen on the characteristic

curve obtained from numerical results presented in Figure 4.

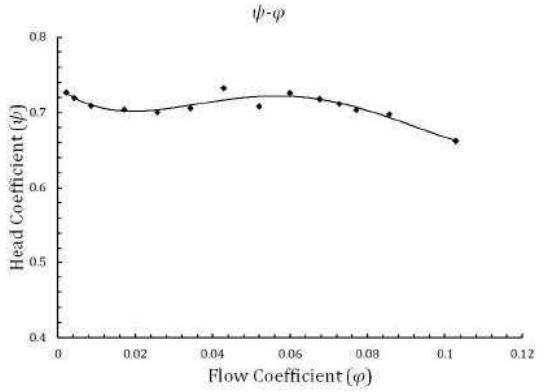

Figure 4 – Head coefficient curve in terms of flow coefficient obtained from numerical results

Figure 5 shows the pump's efficiency curve based on the flow coefficient obtained from numerical solution results. As it can be seen, the pump's maximum efficiency ranges from the flow coefficient of 0.060 to 0.086. The flow coefficient point of 0.077 is the best point of the pump's efficiency based on experimental data of this pump. Curves presented in Figures 3 to 5, i.e., head and efficiency coefficient based on flow coefficient, are the pump's performance characteristic curves in a non-cavitating state.

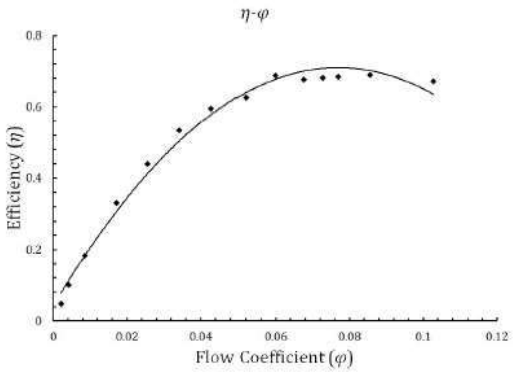

Figure 5 – Efficiency curve in terms of flow coefficient obtained from numerical results

The cavitating characteristic curve of the pump is obtained by decreasing the cavitation number in a fixed flow coefficient. In the present study, the pump's inlet pressure with rotating speed and a fixed flow coefficient was reduced. By gradual reducing of cavitation number, vapor cavities are built in low-pressure areas in the pump and while moving in the flow passage to high-pressure areas are condensed or collapsed. When there is an inducer in the pump, this process occurs in the inducer, and bubbles collapse in the inducer's channels before entering the impeller. So, the fluid enters the impeller with a liquid-phase state and standard pressure.

Figure 6 shows the meridional static pressure distribution inside the pump. As it can be seen, the contours are presented nondimensionally in several cavitation numbers. Cavitating areas are not very obvious because there is a significant difference between the maximum and minimum pressure.

Figure 7 presents the vapor volume fraction contour of different cavitation numbers. As shown in the figures, the smaller the cavitation number becomes, the larger the size of cavity in the pump gets. Although an inducer was added to the pump, a cavity was created on the leading edge of the impeller with the cavitation number of 0.1080. This signifies the importance of inducer presence in that if there is not an inducer added to the pump, the cavitation becomes more malevolent and the size of cavities created at the entrance of impeller larger.

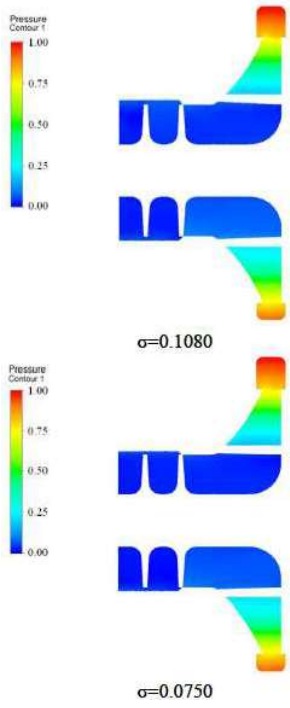

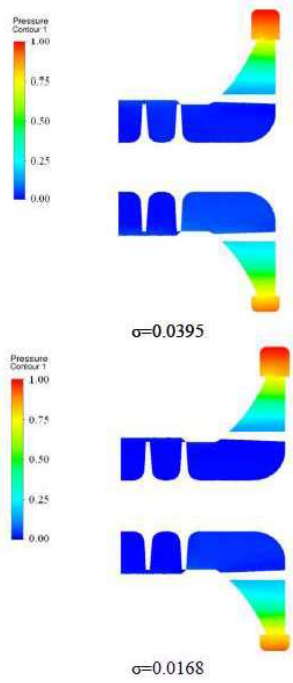

Figure 6 – Static pressure contour on the meridional cross section of the pump

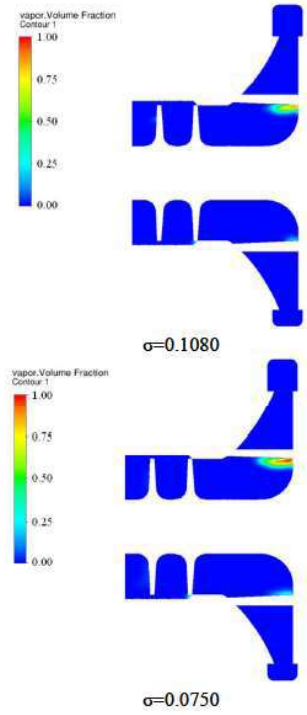

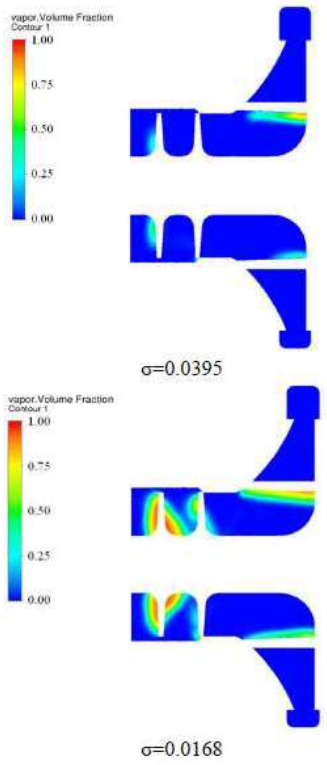

Figure 7 – Volume fraction contour on the meridional cross section of the pump

In Figure 8, the pressure coefficient of one of the impeller blades for different cavitation numbers is presented. The pressure coefficient equals to regional cavitation number ($C_p = -\sigma$). The pressure coefficient is calculated through the equation below based on regional pressure, vapor pressure, density, radius of incucer's blade tip and rotational speed.

$$C_p = \frac{p_v - p}{\frac{1}{2}\rho(r_{t1}\omega)^2}$$

In Figure 8, the symmetry of the pressure coefficient of the blade is demonstrated based on the impeller's non-dimensional radius. *R* denotes the outlet radius of the impeller. As shown in Figure 8, cavitation inception and cavitation numver decrese interrupt the pump's performance. It can be concluded from the following figure that the head of outlet flow from the impeller drops in a cavitating regime.

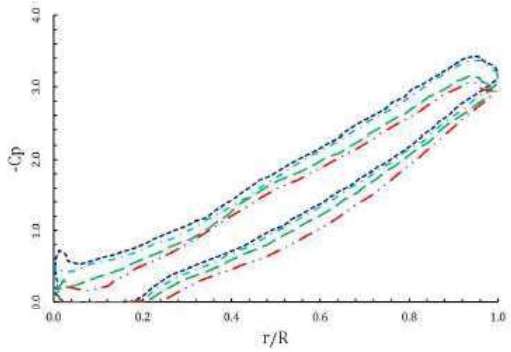

Figure 8 – Distribution of minus pressure coefficient on the one of the impeller blades in the radial direction

Figure 9 shows the cavities in the impeller's axis. As shown in different parts of Figure 9, the size of cavities was largened by the decrease of cavitation number. That is to say, the smaller the cavitation number, the larger the cavity inside the pump. Different parts of Figure 9 show vapor volume fractions for different cavitation numbers. The extension of cavities blocks the flow and declines the pump's performance.

In Figure 10, the pump's cavitation breakdown curve is presented. The head coefficient is drawn based on the cavitation number in this curve. This graph was obtained from the results of numerical analysis on different inlet pressures under a fixed rotation and flow rate. When the inlet pressure is reduced to a certain amount, the pump's head starts to drop. In most bodies of literature, the critical cavitation number is reported to be 3 percent of the head drop. [2] The critical cavitation number obtained from experiments for the pump used in this study equals 0.036 and is shown in red in the graph. However, CFD analyses report the number 0.020 for the critical cavitation number.

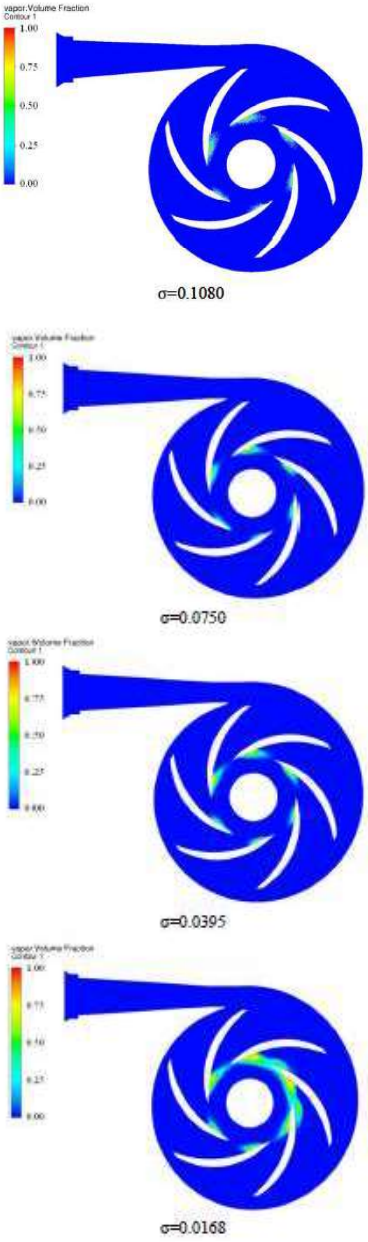

Figure 9 – Volume fraction contour in the view perpendicular to the pump's axis

In Figure 11, cavities of a condition with the fixed vapor volume fraction of 0.5 for two cavitation numbers are shown. In the cavitation breakdown number equaling 0.0168, a large part of the fluid pass channel was occupied by vapor cavities.

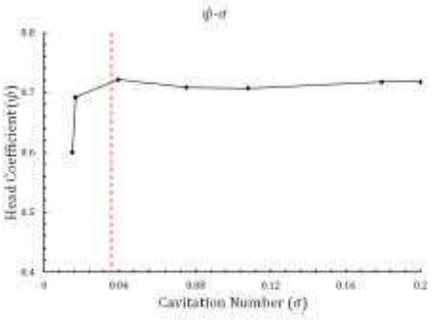

Figure 10 – Pump's cavitation breakdown curve

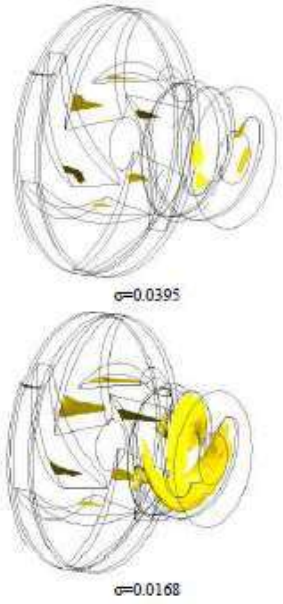

Figure 11 – Cavities inside the pump at two cavitation number

Conclusions

The current study demonstrated the results of simulating cavitating and non-cavitating flow through a high-speed centrifugal pump. First, the pump's characteristic curve of the non-cavitating state outside the design point was obtained and compared to experimental results. Comparisons signified a significant difference between numerical and experimental results.The reasons causing the difference was explained precisely. Thus, the numerical results should be used with caution and be corrected based on experimental results.

In the next step of present study, cavitating flow through the pump was simulated by employing the homogenous multiphase mixture method and the cavitating Rayleigh-Plesset model. Then, the cavitation breakdown curve was obtained, and the critical cavitation number was determined. The critical cavitation number obtained from numerical and experimental results were compared, and the comparison indicated a significant difference between them. Thus, when using numerical analysis results to determine the inlet pressure for ensuring an incessant cavitating performance of the pump and preventing performance decline caused by cavitation inception, a minimum safety factor of 1.8 should be applied.

References

1. Brennen C.E., Hydrodynamics of Pumps, Concepts NREC and Oxford University, 1994.
2. Coutier-Delgosha O., Reboud J. L., Fortes-Patella R., Numerical Study of the Effect of the Leading Edge Shape on Cavitation Around Inducer Blade Sections," JEME International Journal, Series B, Vol. 45, No. 3, 2002.
3. Tokumasu T., Sekino Y., Kamijo K., "The Numerical Analysis of the Effect of Flow Properties on the Thermodynamic Effect of Cavitation," Trans. Japan Soc. Aero. Space Sci., Vol. 47, No. 156, 2004.
4. Ugajin H., Watanabe O., Kawai M., Kobayashi S., Tomaru H., Ohta T., "Numerical Simulation of Cavitating Flow in Inducers," 40th AIAA/ASME/SAE/ASEE Joint Propulsion Conference, Fort Lauderdale, 11-14 July 2004.
5. Pierrat D., Gros L., Pintrand G., Le Fur B., Gyomali Ph., "Experimental and Numerical Investigation of Leading-Edge Cavitation in a Helico-Centrifugal Pump," 12th International Symposium on Transport Phenomena and Dynamics of Rotating Machinery, Honolulu, Hawaii, February 17-22, 2008.
6. Yamamoto K., Tsujimoto Y., "Backflow Vortex Cavitation and Its Effects on Cavitation Instabilities," International Journal of Fluid Machinary and Systems, Vol. 2, No. 1, January-March 2009.
7. Kang D., Yonezawa K., Horiguchi H., Kawata Y,. Tsujimoto Y., "Cause of Cavitation Instabilities in ThreeDimensional Inducer," International Journal of Fluid Machinary and Systems, Vol. 2, No. 3, July-September 2009.
8. An Y. J., Shin B. R., "Numerical Investigation of Suction Vortices Behavior in Centrifugal Pump," Journal of Mechanical Science and Technology, Vol. 25(3), 2011.
9. Somashekar D., Purushothama H. R., "Numerical Simulation of Cavitation Inception on Radial Flow Pump", IOSR Journal of Mechanical and Civil Engineering, Vol. 1, July-August 2012.
10. Campos-Amezcua R., Khelladi S., Mazur-Czerwiec Z., Bakir F., Campos-Amezcua A., Rey R., "Numerical and Experimental Study of Cavitating Flow Through an Axial Inducer Considering Tip Clearance, " Proc ImechE Part A: J Power and Energy, Vol. 227(8), 2013.
11. Mishra A., Ghosh P., "Predicting Performance of Axial Pump Inducer of LOX Booster Turbo-pump of Staged Combustion Cycle Based Rocket Engine Using CFD," IOP Conf. Series: Material Science and Engineering 101, 2015.
12. Guo X., Zhu Z., Cui B., Shi G., "Effects of the Number Blades on the Anti-Cavitation Characteristics and External

Perfomancce of a Centrifugal Pump," Journal of Mechanical Science and Technology, Vol. 30 (7), 2016.
13. Cheraqi A., Ebrahimi R., "Determination of a High-speed Centrifugal Pump's Steady Performance Range by Computational Fluid Dynamics," Scientific-Research Quarterly Journal of Aerospace Science and Technology, Vol. 13, Issue 2, 2021
14. American Petroleum Institute (API), "API 610 Std, Centrifugal Pumps for Petroleum, Petrochemical and Natural Gas Industrie," 10th Edition, 2010.
15. CFX-ANSYS Canada Ltd, Cfx-5.7: "Solver Theory"،Canada, 2004